This item is the archived peer-reviewed author-version of:

Plasma-based CO₂ conversion : to quench or not to quench?

Plasma-Based CO$_2$ Conversion: To Quench or Not to Quench?

Vincent Vermeiren and Annemie Bogaerts[*]

Department of Chemistry, Research group PLASMANT, University of Antwerp,

Universiteitsplein 1, 2610 Antwerp, Belgium

E-mail: annemie.bogaerts@uantwerpen.be

Abstract

Plasma technology is gaining increasing interest for CO_2 conversion. The gas temperature in (and after) the plasma reactor largely affects the performance. Therefore, we examine the effect of cooling/quenching, during and after the plasma, on the CO_2 conversion and energy efficiency, for typical "warm" plasmas, by means of chemical kinetics modelling. For plasmas at low specific energy input (SEI $\sim$ 0.5 eV/molec.), it is best to quench at the plasma end, while for high SEI plasmas (SEI $\sim$ 4 eV/molec.), quenching at maximum conversion is better. For low SEI plasmas, quenching can even increase the conversion beyond the dissociation in the plasma, known as superideal quenching. To better understand the effects of quenching at different plasma conditions, we study the dissociation and recombination rates, as well as the vibrational distribution function (VDF) of CO_2, CO, and O_2. When a high vibrational-translational (VT) non-equilibrium exists at the moment of quenching, the dissociation and recombination reaction rates both increase. Depending on the conversion degree at the moment of quenching, this can lead to a net increase or decrease of CO_2 conversion. In general, however, and certainly for equilibrium plasmas at high temperature, quenching after the plasma helps to prevent recombination reactions and clearly enhances the final CO_2 conversion. We also investigate the effect of different quenching cooling rates on the CO_2 conversion and energy efficiency. Finally, we compare plasma-based conversion to purely thermal conversion. For warm plasmas with typical temperature of 3000-4000 K, the conversion is roughly thermal.

1 Introduction

In order to mitigate the devastating effects of climate change on society, extensive research is carried out on the conversion of greenhouse gases responsible for global warming.[1] Plasma, created by applying electricity to a gas so that a cocktail of reactive species is formed (electrons, ions, radicals, excited species), is of particular interest,[2–4] since it can convert (excess) electrical energy from intermittent renewable energy sources into

chemical energy, it is very flexible, and can be scaled easily. Many different types of plasma reactors are investigated for CO_2 conversion, such as dielectric barrier discharges (DBDs),[5–12] gliding arc (GA) plasmas,[13–15] microwave (MW) plasmas,[16–21] atmospheric pressure glow discharges (APGD),[22,23] and nanosecond-pulsed plasmas.[24–27] MW, GA, APGD and nanosecond-pulsed plasmas yield a better performance than e.g., DBD plasmas.[4] This is generally attributed to the lower reduced electric field (E/N) of 50-100 Td, compared to DBD plasmas (200 Td and above),[2,4,28] which leads to a lower electron temperature (1-2 eV), compared to the latter (3 eV and higher).[29]

At lower electron temperature, more energy goes into vibrational excitation,[2,4] while electrons at higher energies mainly cause electronic excitation, ionization, and direct electron impact dissociation.[4,28,29] The latter explains the lower energy efficiency of DBD plasmas, because direct electron impact dissociation requires at least 7 eV energy, which is considerably greater than the bond energy of CO_2 (5.5 eV), so the extra energy is wasted.[28]

The electron energy that goes into the lower CO_2 vibrational levels in MW, GA and APGD plasmas can either relax to heat in so-called vibrational-translational (VT) relaxation,[2,4,30,31] or undergo so-called vibrational-vibrational (VV) relaxation, in which CO_2 molecules can acquire more vibrational energy. This process is called vibrational ladder climbing, and proceeds until the vibrational energy of the CO_2 molecules reaches the dissociation limit.

Over the last few years, research on CO_2 plasmas was largely focussed on increasing the energy efficiency of CO_2 conversion. A lot of attention was paid to increasing the VT non-equilibrium.[28,29,32–37] The aim was to enhance the vibrational temperature without (significantly) raising the gas temperature. However, in most experiments conducted with MW, APGD and GA discharges, the plasma appears to be in (or close to) thermal equilibrium, with the gas temperature (nearly) equal to the vibrational temperature.[15,19,21,23,31,38,39]

These high gas temperatures (i.e. > 3000 K[18,21,40]) can even be reached at relatively

3

low specific energy inputs (SEI), because the power input is localized in a limited gas volume[20,38,40] leading to a much higher local SEI.[20] This phenomenon is especially pronounced in APGD, GA and MW plasmas. In APGD and GA plasmas the contracted nature is inevitable, since the discharge is characterized by a plasma column that connects two electrodes.[2,15,38] In MW plasmas, the discharge is known to radially contract with increasing pressure, starting from around 100 mbar,[39–41] in which the minimal plasma radius is equal to the skin depth.[40]

The high temperatures[15,18–21,38,40] lead significant thermal dissociation at the expense of vibrational-induced dissociation. The vibrational distribution function (VDF) exhibits a Boltzmann distribution, with no overpopulation of the higher vibrational levels, and the dissociation mainly occurs from the lower vibrational levels of CO_2.[31,38] While high energy efficiencies can be reached at these temperatures,[21,38,39,42] the overall conversion starts to become constrained by the recombination reactions, mainly of CO with O_2 molecules, which become more important at higher temperatures.[31,38,39]

A possible pathway to limit these recombination reactions at high gas temperatures is by quickly cooling the gas, thereby quenching the converted reaction products. Experimentally, this can be accomplished by a sharp temperature gradient between the plasma core and the surrounding gas.[14,20] In addition, the gas can be cooled by enhanced radial heat transport, achieved in turbulent flow regimes,[39,43,44] or by supersonically accelerating the gas.[17] For high SEI plasmas, however, in which more than 0.19 eV/molec. goes to heat, this acceleration has to take place in the afterglow to prevent thermal choking of the flow.[2,45]

Next to limiting the recombination reactions, and thus freezing of the reaction products (so-called ideal quenching), it is also possible to increase the CO_2 conversion upon quenching. This is called super-ideal quenching and happens when a VT non-equilibrium, created or enhanced by the sudden drop in gas temperature, promotes VV relaxation to the higher vibrational levels, and further enhances the dissociation reactions. More specif-

ically, this can happen by the reactions of vibrationally excited CO_2 molecules with any molecule (M), or with an O atom (i.e. $CO_2 + M \rightarrow CO + O + M$, or $CO_2 + O \rightarrow CO + O_2$).

Although it has been experimentally and theoretically demonstrated that high energy efficiencies for CO_2 conversion can be reached in warm plasmas at temperatures of 3000 K and above,[18–21,38,42] and it is often stated that quenching is promising to reach higher energy efficiencies,[2,17,20,31,39] more insight is needed to demonstrate its full potential. Therefore, we examine here the effect of quenching on the CO_2 conversion and energy efficiency for different plasma conditions. Furthermore, we compare the plasma conversion with purely thermal conversion, for the same power input, to elucidate the difference in performance, and to determine the actual role of thermal dissociation in plasma-based CO_2 conversion.

2   Model Description

2.1   Plasma Model

We apply a zero-dimensional (0D) chemical kinetics model, using ZDPlasKin.[46] This model solves the continuity equation for the different plasma species

$$\frac{dn_s}{dt} = \sum_j R_j[a_{sj}^R - a_{sj}^L] = \sum_j (k_j \prod_l n_l)[a_{sj}^R - a_{sj}^L] \tag{1}$$

in which index j refers to reaction j and index l refers to the different reactants of reaction j. a_{sj}^R and a_{sj}^L are the right- and left-hand side stoichiometric coefficients of species s, respectively, taking part in reaction j, k_j is the reaction rate coefficient, and $R_j = k_j \prod_l n_l$ is the reaction rate, with $\prod_l n_l$ the product of densities n_l of species present on the left side of reaction j.

Within the ZDPlasKin framework, a chemical kinetics solver is coupled to the Boltzmann solver BOLSIG+,[47] to calculate the electron energy distribution function (EEDF)

using a set of cross sections, corresponding to the reactions listed in Table S1 of the supporting information (SI), including superelastic collisions. The EEDF is regularly updated during the simulations, upon changes in the chemical composition, reduced electric field, or gas temperature.

2.2 Chemistry Set

The species in our model are listed in Table 1. The chemistry set is a slightly reduced form of other sets used in the past.[28,48–50] The effect of the chemistry reduction on the model results was examined in ref. 31. This reduced chemistry set has been used in more recent work,[29,45,49,51] including an uncertainty analysis[49] in which it was argued that more species had a negative impact on the model uncertainty, while they virtually had no influence on the model results.

Given the importance of vibrational ladder climbing in studying the role of thermal (equilibrium) vs non-equilibrium CO_2 dissociation, we include all (21) asymmetric mode vibrational levels, up to the dissociation limit, as well as the four (degenerate) lowest symmetric mode vibrational levels, which include both the bending and symmetric stretch mode (see Table 1). The choice to only include these few symmetric mode levels is justified, since for $E/N > 20$ Td, and thus at the conditions under study here , primarily the asymmetric mode is excited,[52,53] and experiences a very fast VV relaxation.[28,51] For CO and O_2, 50 and 33 levels are taken into account, respectively. For O_2, these levels again reach the dissociation limit. For CO, there are 63 levels up to the dissociation limit, but the levels above 50 were neglected, as they did not affect our results, due to the low vibrational excitation and strong VT relaxation, leading to a low population.

The full set of reactions in our model can be found in the SI (Tables S1-S5), and includes electron impact, ion-ion, neutral-neutral reactions, and VT and VV relaxation between different molecules.

All reactions in this chemistry set are characterized by an individual uncertainty. While

these uncertainties will have an impact on specific calculation results, such as the CO_2 conversion, the trends predicted are typically not affected by these uncertainties.[49] Note that this quoted study only applied to gas temperature up to 2000 K, and the effect of the uncertainties on the neutral reactions can lead to higher deviations at the higher temperatures considered here. We therefore focus more on the overall trends, rather than on the absolute values of e.g., CO_2 conversion and energy efficiency.

Most of the rate coefficients and cross sections are generally known for the ground state or low vibrational level molecules. Scaling laws are used to scale these rate coefficients towards higher vibrational levels. To determine the various rate coefficients, we mostly follow the same approach as in previous work,[28,29,31,45,48–51,54] with an additional correction term on the rates, scaled with the Fridman Macheret α model. This is explained in more detail in the SI.

2.3 Modelling Approach

We follow the time-evolution of a volume element as it moves through a plasma reactor. The model starts with pure CO_2, mimicking the gas at the inlet of the reactor, and a Boltzmann vibrational distribution, corresponding to 300 K, i.e., the gas temperature at the inlet. At t=0, plasma power is applied to the gas (or thermal power when we use the model for pure thermal conversion; see below).

At any time during the simulation, the ideal gas law is applied. We assume that pressure remains constant, so the volume element considered can expand or contract upon changes in the gas temperature, or upon changing chemical composition (e.g., 1 CO_2 molecule is converted into CO and O, thus increasing the number of species). We take this effect into account by introducing a gas expansion factor, $\beta(t)$, which equals 1 at the start of the simulation, and drops when the gas expands. The factor is defined as:

$$\beta(t) = \frac{M(t=0)T_g(t=0)}{M(t)T_g(t)} \tag{2}$$

7

Table 1: Species described in the model.

Neutral ground state species
CO_2, CO, O_2, O, C

Charged species
CO_2^+, CO^+, O_2^+, CO_4^+, O^-, O_2^-, CO_3^-, CO_4^-, e^-

Excited states	Associated energy [eV]	State[a]
$O_2[v_{1-33}]$	Anharmonic oscillator	
$CO[v_{1-50}]$	Anharmonic oscillator	
$CO_2[v_{1-21}]$	Anharmonic oscillator	(00n)
$CO_2[v_a]$	0.083	(010)
$CO_2[v_b]$	0.167	(020) + (100)
$CO_2[v_c]$	0.252	(030) + (110)
$CO_2[v_d]$	0.339	(040) + (120) + (200)
$CO_2[e_1]$	10.5	$(^1\Sigma_u^+) + (^3\Pi_u) + (^1\Pi_u)$
$O_2[e_1]$	0.98	$(a^1\Delta_g)$
$O_2[e_2]$	1.6	$(b^1\Sigma_g^+)$
$O_2[e_3]$	4.5	$(A^3\Sigma_u^+) + (C^3\Delta_u) + (c^1\Sigma_u^-)$
$O_2[e_4]$	9.7	radiative levels
$O_2[e_5]$	14.7	radiative levels
$CO[e_1]$	6.22	$(a^3\Pi_r)$
$CO[e_2]$	6.8	$(a'^3\Sigma^+)$
$CO[e_3]$	7.9	$(A^1\Pi)$
$CO[e_4]$	10.4	$(b^3\Sigma^+)$
$CO[e_5]$	10.6	$(C^1\Sigma^+) + (E^1\Pi)$
$CO[e_6]$	13.5	$(d^3\Delta_i) + (e^3\Sigma^-)$

[a] CO_2 electronic states designation from Grofulović et al.,[53] O_2 and CO electronic states notation from Itikawa.[55]

with M the total number of molecules, and T_g the gas temperature. For example, if all CO_2 is dissociated into CO and $\frac{1}{2}O_2$, the initial number of molecules M(t=0) rises to $\frac{3}{2}$M(t=0), and thus $\beta = \frac{2}{3}$, at constant gas temperature, because the volume expands to keep the pressure constant. Similarly, the expansion factor drops upon rising gas temperature. The electron density is not included in this expansion factor, as the ionization degree is too small.

The plasma conditions are defined in the model by setting a certain ionization degree (d_i). The electron density (n_e) then equals $d_i \times N$ (with N the gas number density). At the same time, a constant (DC) reduced electric field E/N (with E the electric field) is set. The deposited power density (in eV/cm^{3}s) applied to the plasma is then calculated using Joule's law:

$$P_{dep,pl} = \sigma E^2 = \sigma N^2 \left(\frac{E}{N}\right)^2 \tag{3}$$

with σ the conductivity (in $\frac{C}{cmVs}$), given by $\sigma = en_e\mu_e$. The electron mobility μ_e is obtained from the Boltzmann solver, and e is the elementary charge.

In order to compare the plasma performance with pure thermal simulations, we apply a heat source term with the same power deposition profile $P_{dep,th}$ as in the plasma case:

$$\frac{N_{th}}{\beta_{th}}P_{dep,th} = \frac{N_{pl}}{\beta_{pl}}P_{dep,pl} \tag{4}$$

with N_{th} and β_{th} being the total gas number density and expansion factor of the thermal simulation, respectively, and N_{pl} and β_{pl} for the plasma simulation.

At time t = 0 s, the plasma is ignited by applying the power as described above. The plasma is sustained until the applied power reaches the value corresponding to a certain predefined SEI (in eV/molec.), defined as:

$$SEI = \frac{\int_0^t \frac{P_{dep}(t)}{\beta(t)}dt}{N(t=0)} \tag{5}$$

9

Note that the dependency between the SEI and the residence time is specific to the conditions under study. In reality, a similar SEI can be reached with different deposited power profiles, leading to a different deposited power density. When the power density is lower, the residence time will increase. However, this situation will correspond to lower ionization degrees or reduced electric fields, and we decided to keep these fixed in our study, as characteristic plasma parameters. Also, in a 0D model, the plasma parameters are assumed to be homogeneous. In reality, localized power deposition can also lead to longer residence times for the same total SEI.[20]

We aim to study the effect of quenching at conditions of maximum CO_2 conversion and energy efficiency. This is typically achieved in MW plasmas at intermediate pressure.[19,21] We therefore assume a fixed pressure of 100 mbar. The CO_2 conversion is calculated as

$$X(t)[\%] = \left[1 - \frac{N_{CO_2}(t)}{\beta(t)N_{CO_2}(t=0)} \right] \times 100\% \tag{6}$$

where N_{CO_2} is the total number density of all CO_2 molecules (i.e. the sum of the ground state and all vibrationally and electronically excited CO_2 molecules) at a given time t.

The energy efficiency is calculated as

$$\eta[\%] = X[\%] \frac{\Delta H^o}{SEI} \tag{7}$$

where ΔH^o = 2.93 eV/molec. is the reaction enthalpy of the reaction $CO_2 \rightarrow CO + \frac{1}{2}O_2$ at the inlet temperature of 300 K.

At the plasma conditions under study, not all the applied power is used for CO_2 conversion, but a significant fraction is released as heat. In our model, the gas temperature is calculated self-consistently according to:

$$N\frac{\gamma k_B}{\gamma - 1}\frac{dT_g}{dt} = P_{el} + \sum_j R_j \Delta H_j - P_{ext} \tag{8}$$

with $\gamma = c_p/c_v$ the ratio of specific heats that is regularly updated depending on the concentration of the different species, P_{el} the gas heating power density due to elastic electron-neutral collisions, ΔH_j the heat released (or consumed) by each reaction j, and P_{ext} the power loss density due to exchanges with the surroundings.

The heat exchange with the surroundings is particularly important in order to tune the (non) equilibrium effects. The external cooling term is defined as:[31,50]

$$P_{ext} = c\frac{8\lambda(T_g)}{R^2}(T_g - T_w) \tag{9}$$

where λ is the gas thermal conductivity, T_w is the wall temperature (assumed as 300 K), and the reactor radius R is set to 7 mm.[56,57] The gas thermal conductivity is calculated by:[50,58] $\lambda(T_g) = (0.071T_g - 2.33) \times 10^{-3}Wm^{-1}K^{-1}$.

In order to study the effect of quenching on the CO_2 dissociation, we added a tuning constant c, to increase or decrease the cooling power (or thermal conductivity), which determines the gas temperature. Without quenching, c remains the same during the entire simulation. The gas can be quenched by dropping the gas temperature to 300 K (i.e. instantaneous quenching), or by increasing the cooling constant (i.e. c_1 before quenching and c_2 after quenching).

In reality, the cooling by thermal conductivity can be increased by gas flow turbulence.[16,44] A rise in thermal conductivity by a factor 100 (which is our model corresponds to c = 100) is quite feasible for CO_2 at room temperature. Indeed, while in our model, the thermal conductivity at 300 K is 0.019 W/(m*K), the effective thermal conductivity due to turbulence at 300 K was estimated to be 1-3 W/(m*K),[16] hence a factor (c=) 100 higher. The highest cooling constant in our model is c = 1000, which probably may only be realized upon mixing with a cold gas. However, the latter could also result in changes

in the gas composition, but these effects are beyond the scope of our study. Indeed, our study is more conceptual.

3 Results and Discussion

All results are presented for a pressure of 100 mbar, which typically yields high energy efficiencies.[4] The ionization degree (d_i) is set to 10^{-6}, which can be considered as a lower value for diffuse microwave plasmas,[40] but could also be applicable for glow discharge plasmas.[59] The reduced electric field (E/N) is set to 50 Td, as this is a value that ensures high vibrational exciation of the assymetric mode levels of CO_2. We also present the results for an ionization degree (d_i) of 10^{-4} and E/N of 100 Td, to illustrate the behavior in a wider range of conditions.

3.1 Effect of Cooling Constant on the CO_2 Conversion, Gas and Vibrational Temperature During Plasma

Fig. 1 shows the time-evolution of the CO_2 conversion (left axis) and gas and vibrational temperature (right axis) for a plasma with SEI = 5 eV/molec., at weak (a) and strong (b) cooling, hence, representing a VT-equilibrium (or warm) plasma and a non-equilibrium (or cold) plasma, respectively. The vertical lines indicate the times at which an SEI of 1, 2, 3, and 4 eV/molec. is reached. Note that the residence time to reach a certain SEI in the cold plasma is shorter than in the warm plasma, as the gas density (N) is higher, requiring a higher electric field (and thus higher SEI) to reach an E/N of 50 Td.
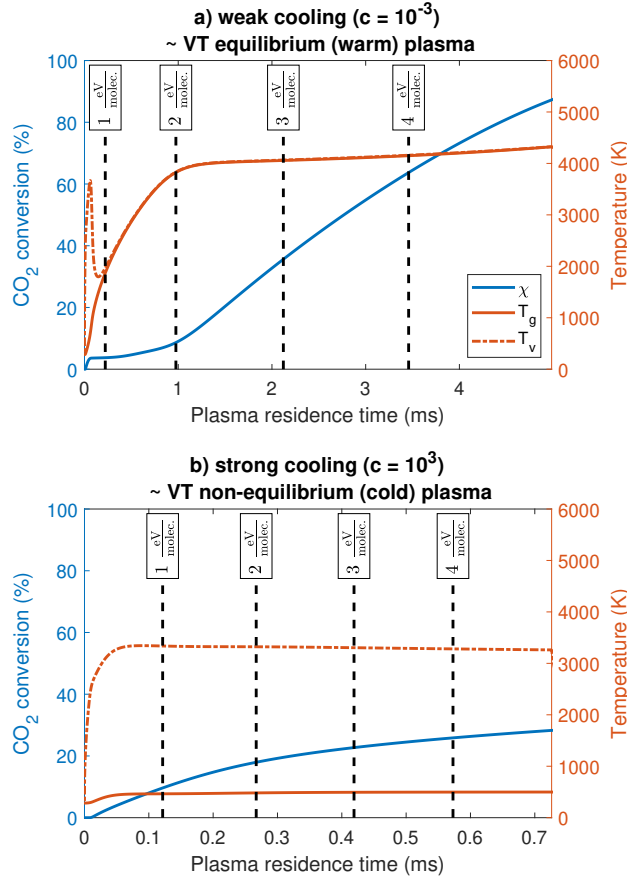
Figure 1: Time-evolution of the CO_2 conversion (left axis) and gas and vibrational temperature (right axis) for a plasma with SEI of 5 eV/molec., and for (a) weak cooling (c = 10^{-3}) and (b) strong cooling (c = 10^3), mimicking VT equilibrium (or warm) plasma and non-equilibrium (or cold) plasma, respectively. The time after which 1, 2, 3, and 4 eV/molec. of energy is supplied to the plasma is indicated with vertical dashed lines.

At weak cooling (fig. 1 (a)), a non-equilibrium between the vibrational and gas temperature arises at the start of the plasma, but quickly disappears, since the gas temperature rapidly rises, thus enhancing VT relaxation, so that the vibrational energy is lost to heat. At an SEI of 1 eV/molec., the vibrational and gas temperature are already in equilibrium. Van den Bekerom et al.[60] and Klarenaar et al.[32] also demonstrated experimentally for MW plasmas and glow discharge plasmas, respectively, that the non-equilibrium between vibrational and gas temperature is largest at the onset of plasma, after which it decreases when higher gas temperatures are reached. Exact comparison is not possible, as these experiments were performed at pressures of 25 mbar and 6.7 mbar, respectively.

The CO_2 conversion increases slowly at the plasma onset. It reaches 3.7 % at 1 eV/molec., and 8.6 % at 2 eV/molec., but then it rises much faster. At this time, the gas temperature has reached 3820 K, resulting in strong thermal dissociation of CO_2.[38,42] Thus, this high gas temperature is needed for significant conversion. At 5 eV/molec. a conversion of 84.6% is reached.

At strong cooling (fig. 1 (b)), a non-equilibrium between vibrational and gas temperature exists for all shown SEI values, since VT relaxation is much less important at low gas temperatures. At an SEI of 1 eV/molec., the CO_2 conversion reaches 9.5 %, which is more than double of what was reached at the same SEI in fig. 1 (a). However, when the SEI is higher than 2 eV/molec., the CO_2 conversion rises much more slowly than in fig. 1 (a). At 5 eV/molec., a CO_2 conversion of 28.3 % is reached, hence much lower than in fig. 1 (a). Thus, at SEI values below or equal to 1 eV/molec., cooling of the plasma is beneficial for the conversion, consistent with previous studies performed by our group.[29] For SEI values of 2 eV/molec. and higher, cooling is detrimental, pointing towards the important role of thermal dissociation. This will be further elaborated in section 3.7.

3.2 CO_2 Conversion and Gas Temperature in the Afterglow of Warm Plasmas

In fig. 2, we plot the time-evolution of the conversion and gas temperature in the afterglow of a plasma with SEI of 1, 2, 3, 4, and 5 eV/molec., at weak cooling (c = 10^{-3}), i.e., the afterglow of fig. 1 (a), starting at the different vertical dashed lines.
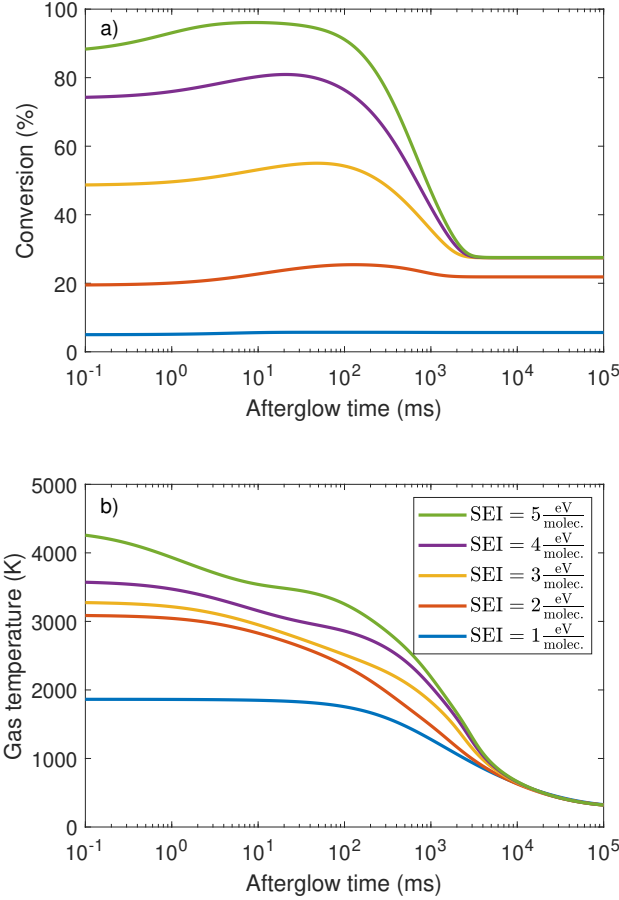
Figure 2: Time-evolution of the CO_2 conversion (a) and gas temperature (b) in the afterglow of a warm plasma with SEI of 1, 2, 3, 4, and 5 eV/molec., at weak cooling ($c = 10^{-3}$), when no additional cooling is applied in the afterglow.

The conversion continues to rise in the afterglow, due to thermal CO_2 dissociation. This is most obvious for larger SEI, and thus a higher gas temperature. Indeed, the system may not yet be in chemical equilibrium, because of the short residence time. At lower ionization degrees and reduced electric fields, when the residence time to reach these SEI values is longer, this equilibrium can already be reached inside the plasma.

Next to thermal dissociation, recombination is also important at high gas temperatures.[31] In the afterglow, the temperature slowly decreases as a function of time (fig. 2 (b)), and around 10-100 ms (depending on the SEI) thermal dissociation becomes less important than recombination, so the CO_2 conversion starts to drop (fig. 2 (a)). After ca. 2 s, the gas temperature has become low enough (ca. 1000-1500 K) for both recombination

15

and dissociation to become unimportant. At that point, the conversion remains constant.

This figure clearly illustrates that when no additional cooling is applied in the afterglow, the CO_2 conversion, although being very high inside the plasma at high SEI values (even close to 100 %), eventually drops to low values ($\sim$ 20-25 %) after a few seconds, due to recombination reactions. To avoid this detrimental effect, we need to apply cooling in the afterglow, to quench the reaction products. This will be studied in the following sections.

3.3   Instantaneous Quenching

Instantaneous quenching, i.e., quickly reducing the gas temperature to 300 K, can prevent the recombination. Indeed, at 300 K, thermal dissociation and recombination are not important, and the converted reaction products are "frozen".

We describe here the effect of instantaneous quenching, (i) at the plasma end, and (ii) in the afterglow, when the CO_2 conversion reaches its maximum without any quenching (see fig. 2).

3.3.1   Quenching After Warm Plasmas

In fig. 3, we plot the time-evolution of the CO_2 conversion (top panels) and gas temperature (bottom panels) for a plasma with SEI of 0.5 eV/molec. (left panels) and 4 eV/molec. (right panels), at weak cooling (c = 10^{-3}). Note that a VT equilibrium exists at the plasma end with SEI of 4 eV/molec., but not at 0.5 eV/molec. (cf. fig. 1 (a)).
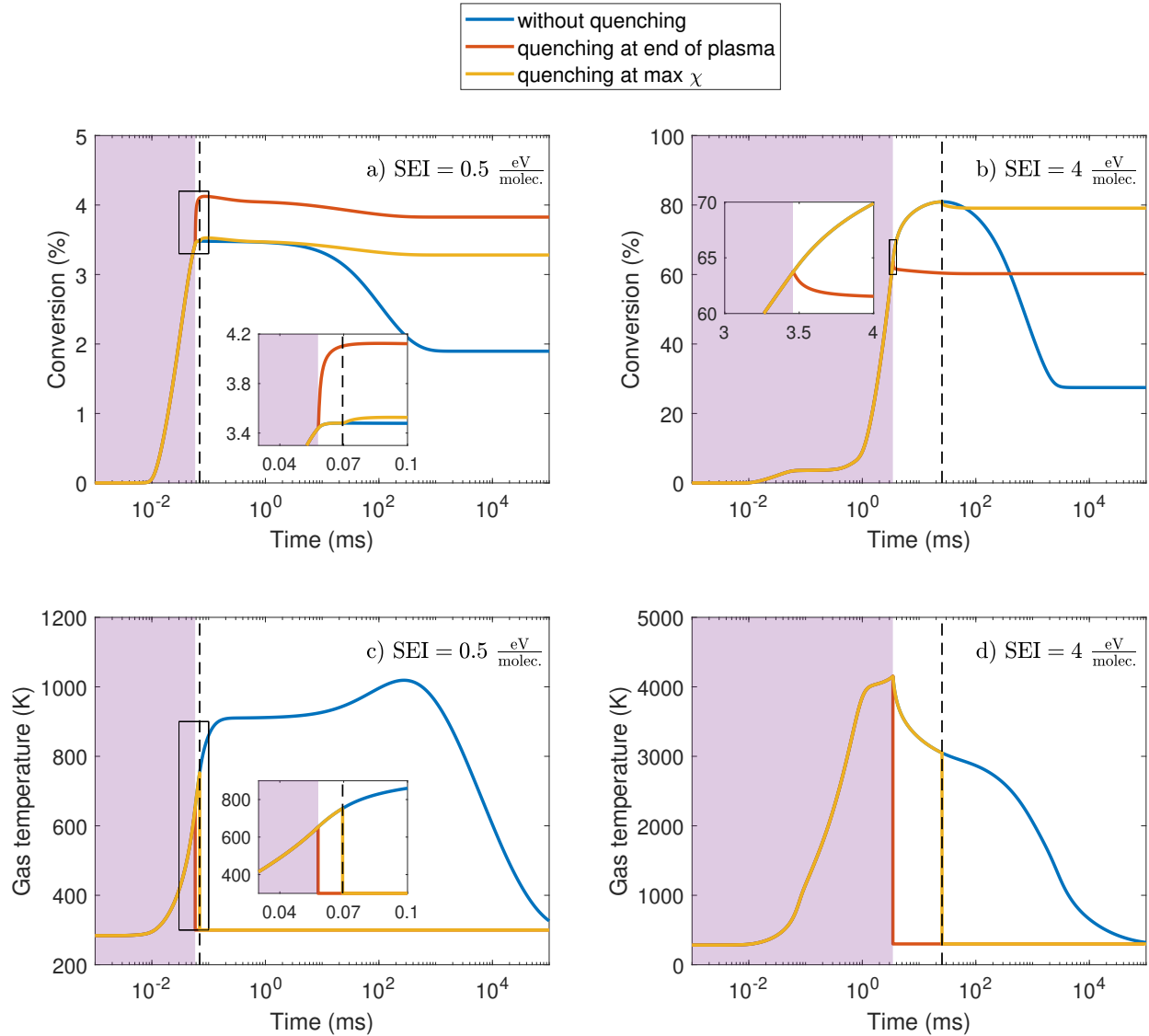
Figure 3: Time-evolution of the CO_2 conversion (a and b) and gas temperature (c and d) without quenching (blue curve) and with quenching at the plasma end (red curve) and at the maximum conversion in the afterglow (yellow curve) for a plasma with SEI of 0.5 eV/molec. (a and c) and 4 eV/molec. (b and d), at weak cooling (c = 10^{-3}). The purple area indicates the plasma, and the vertical dashed line shows where the conversion reaches a maximum in the afterglow without quenching. Note that the plasma with SEI of 0.5 eV/molec. is characterized by VT non-equilibrium, while SEI of 4 eV/molec. yields a VT equilibrium at the plasma end.

Quenching clearly leads to a higher final CO_2 conversion in all cases, but the ideal quenching moment is different for the plasma with high or low SEI.

For an SEI of 0.5 eV/molec. (fig. 3 (a) and (c)), the optimal quenching moment is at

the plasma end. The conversion increases rapidly after quenching, due to the VT non-equilibrium, enhanced by the fast drop in gas temperature. This is called "super-ideal quenching". Quenching at maximum conversion also yields a higher CO_2 conversion, but since the vibrational temperature drops quickly after switching off the plasma,[51] the VT non-equilibrium, and thus the increase in conversion, is much smaller than when quenching at the plasma end (cf. yellow and red curve in fig. 3 (a)).

For an SEI of 4 eV/molec., the optimal quenching moment is at maximum conversion. Since a chemical equilibrium is not yet reached at the plasma end, the conversion further increases after the plasma (see also fig. 2). For both quenching cases, the CO_2 conversion remains more or less frozen (except for a small drop immediately after quenching). The VT non-equilibrium created by the drop in gas temperature is not enough to give a rise in conversion (i.e. super ideal quenching). The different trends in CO_2 conversion upon quenching, for the two SEI values, will be discussed more in depth in the following sections.

Next to the conversion, the energy efficiency is a good measure for effectiveness of quenching. Fig. 4 summarizes both the conversion and energy efficiency as a function of SEI, without quenching (blue bars), and in case of quenching at the plasma end (red bars) and at maximum conversion (yellow bars).
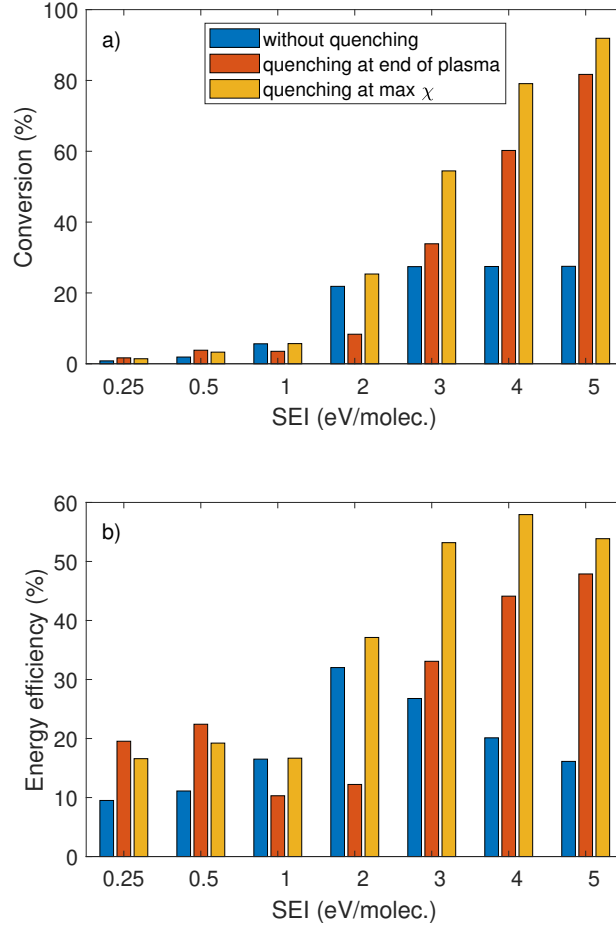
Figure 4: CO_2 conversion (a) and energy efficiency (b) as a function of SEI, without quenching (blue curve), and with quenching at the plasma end (red curve) and at maximum conversion (yellow curve), for warm plasma conditions (i.e. weak cooling; $c = 10^{-3}$). Note that an SEI of 0.25 and 0.5 eV/molec. yields a VT non-equilibrium plasma, while an SEI of 1 eV/molec. and higher results in a VT equilibrium plasma (cf fig. 1 (a))

For all SEI values, quenching at maximum conversion enhances the final conversion and energy efficiency, compared to no quenching. The rise is most pronounced for higher SEI values, where the conversion is most affected by a gradual drop in gas temperature (fig. 2). Our model predicts a maximum final conversion of 90 %, for quenching at maximum conversion, at an SEI of 5 eV/molec., and a maximum energy efficiency of 58 %, again for quenching at maximum conversion, but at an SEI of 4 eV/molec.

Quenching at the plasma end only enhances the final conversion and energy efficiency for SEI below 1 eV/molec. and above 2 eV/molec. For SEI below 1 eV/molec., the VT

19

non-equilibrium at the plasma end, further enhanced upon quenching, yields super-ideal quenching, see also fig. 3 (a)). For SEI values of 1 and 2 eV/molec., the gas temperature at the plasma end is high enough to allow thermal CO_2 dissociation, but there is no significant drop in conversion in the afterglow due to gradual cooling (cf. fig. 2 (a)), because the CO_2 conversion is limited, and thus the recombination reactions are not so important as for higher SEI values. Hence, quenching does not play such a big role in reducing the eventual drop in CO_2 conversion. For higher SEI values, the drop in CO_2 conversion is very pronounced (see fig. 2 (a)), thus explaining why quenching at the plasma end is again beneficial for SEI values above 2 eV/molec.

3.3.2 Quenching After Cold Plasmas

When strong cooling ($c = 10^3$) is applied, the VT non-equilibrium does not disappear for higher SEIs (see fig. 1 (b)). Fig. 5 shows the effect of different quenching times on the evolution of the CO_2 conversion, for a cold plasma with SEI of 4 eV/molec.
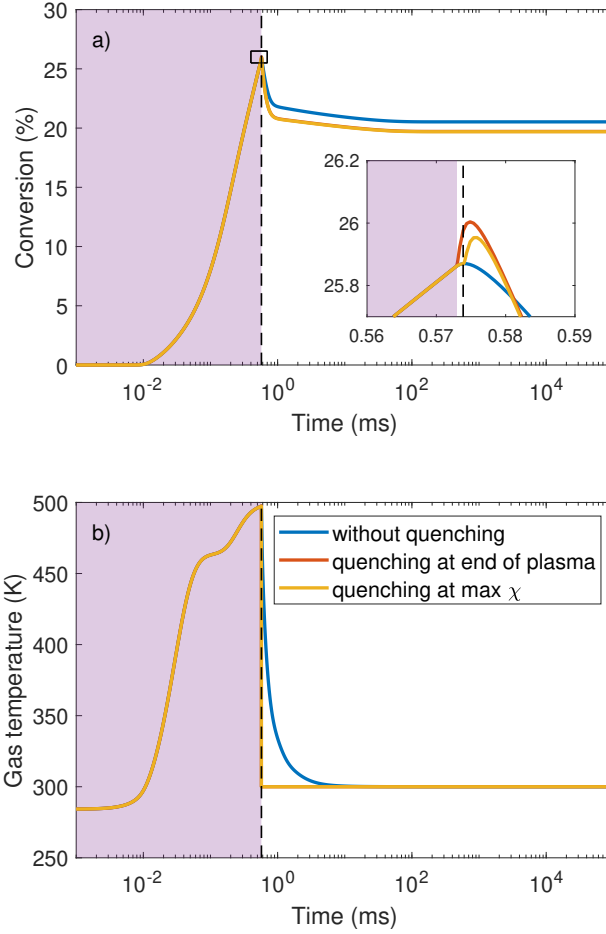
Figure 5: Time-evolution of the CO_2 conversion (a) and gas temperature (b) without quenching (blue curve), and with quenching at the plasma end (red curve) and at the maximum conversion (yellow curve), for a cold (VT non-equilibrium) plasma at SEI of 4 eV/molec. (strong cooling, $c = 10^3$). The purple area indicates the plasma, and the vertical dashed line shows where the conversion reaches a maximum in the afterglow without quenching.

In both cases, the CO_2 conversion slightly rises after quenching (i.e. super-ideal quenching; see inset in fig. 5 (a)), but it is followed by a larger drop compared to without quenching. Hence, the final CO_2 conversion is lower for both quenching options than without quenching.

Comparing this situation to fig. 3 (a), it seems that a VT non-equilibrium can enhance the CO_2 conversion, but for high SEI values, the conversion after plasma is higher, and more recombination can take place, resulting in a lower final CO_2 conversion. Only at low

21

SEI values, non-equilibrium plasmas seem to benefit from quenching, yielding a clearly higher final CO_2 conversion (see fig. 3 (a)).

3.4   Effect of Instantaneous Quenching on the Dissociation and Recombination Rates

To explain the different behavior of instantaneous quenching at low and high SEI, we now discuss its effect on the dissociation and recombination rates, both for a plasma with low and high SEI (0.5 and 4 eV/molec.), characterized by VT non-equilibrium and equilibrium at the plasma end, respectively. Figs. 6 and 7 show the total contribution of the three most important dissociation reactions (reaction X4 in Table S1 of the SI, and reaction N1 and N2 in Table S4) and recombination reactions (N4 and N5 in Table S4 of the SI), to the CO_2 conversion, plotted as positive and negative conversion. For both cases, the quenching moment that provides maximum CO_2 conversion (i.e. quenching at the plasma end for an SEI of 0.5 eV/molec., and quenching at maximum conversion in the afterglow for an SEI of 4 eV/molec., respectively) will be compared with the non-quenched case. Fig. S1 and S2 from the SI show the corresponding time-evolution of these rates after quenching, while fig. S3 and S4 show the evolution of the O radical density after quenching.

Fig. 6 illustrates that the dissociation rates increase upon quenching, as well as the recombination rate by reaction N5. However, due to the low conversion degree (3-4%), little CO and O_2 are present, and this reaction is not important. The main reason for the higher final CO_2 conversion is the lower contribution from recombination reaction N4, due to the faster drop in O radical density, shown in figure S3 from the SI.
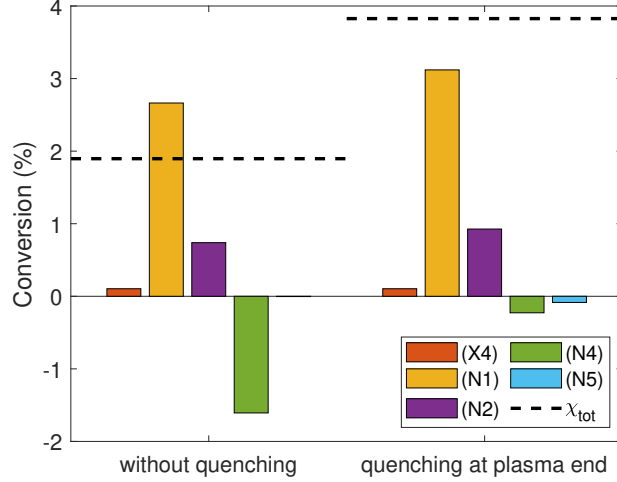
22

Figure 6: Total contribution of the dissociation and recombination reactions to the conversion for a warm VT non-equilibrium plasma with SEI of 0.5 eV/molec. that is quenched at the plasma end (right), and that was subjected to weak cooling (c = 10^{-3}). The case without quenching (left) is shown as a reference. The horizontal dashed lines indicate the final CO_2 conversion. Besides the major dissociation reactions (N1, N2), also electron impact dissociation (X4; see Table S.1 in SI) has a minor contribution.

Fig. 7 illustrates that dissociation reactions N1 and N2, as well as recombination reactions N4 and N5, are all reduced. The reduction is most drastic for N2 and N5. Note that for these two reactions, the conversion value is higher than 100 % in the case without quenching, since on average, CO_2 dissociates and recombines multiple times, but the overall net conversion is of course not above 100 %. Due to the stronger reduction in recombination rate, the final CO_2 conversion increases, as also observed in fig. 3 (b) (yellow vs blue curve). However, fig. S2 in the SI shows that upon quenching, both recombination reactions see a fast but short increase, with respect to the non-quenched case. This can be correlated with the short decrease in CO_2 conversion, that is noticed when quenching (see yellow vs blue curve in fig. 3 (b)).

In the SI, we show the time-evolution of the dissociation and recombination rates (fig. S5), and the contribution of these reactions to the overall CO_2 conversion (fig. S6), for a non-equilibrium cold plasma with SEI of 4 eV/molec. (i.e., strong cooling, c = 10^3) corresponding to fig. 5, in case of quenching at the plasma end. Quenching again enhances the dissociation reactions and recombination reaction N5, similar to figs. 6 and S1 of the
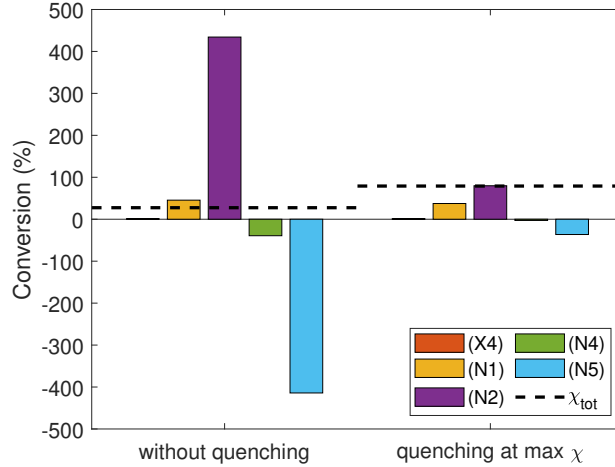
23

Figure 7: Total contribution of the dissociation and recombination reactions to the conversion for an equilibrium plasma with SEI of 4 eV/molec. that is quenched at maximum conversion (right), and that was subjected to weak cooling (c = 10^{-3}). The case without quenching (left) is shown as a reference. The horizontal dashed lines indicate the final CO_2 conversion. In contrast to the non-equilibrium plasma of fig. 6, electron impact dissociation (X4) has a negligible contribution to the final CO_2 conversion.

SI (i.e., VT non-equilibrium warm plasma at SEI of 0.5 eV/molec). However, since the CO_2 conversion is higher than at SEI of 0.5 eV/molec., the recombination reactions are more important, and the rise in recombination reaction N5 happens over a longer time, resulting in an overall drop in CO_2 conversion, as indeed observed in fig. 5.

3.5 Effect of Instantaneous Quenching on the VDFs of CO_2, CO and O_2

The dissociation reactions N1 and N2, and the recombination reaction N5 all have a high activation energy (see Table S4 in the SI). At low gas temperatures, i.e., after quenching, these reactions can only take place if the molecules have sufficient vibrational energy to overcome the activation energy. Therefore, figures 8 and 9 illustrate the VDFs of CO_2, CO and O_2 at different times after quenching, for a VT non-equilibrium warm plasma with SEI of 0.5 eV/molec. that is quenched at the plasma end (cf. fig. 6, fig. S1 in the SI, and red curve in fig. 3 (a)), and an equilibrium warm plasma with SEI of 4 eV/molec. that is quenched at maximum conversion (cf. fig. 7, fig. S2 of the SI, and yellow curve in fig. 3 (b)), respectively.
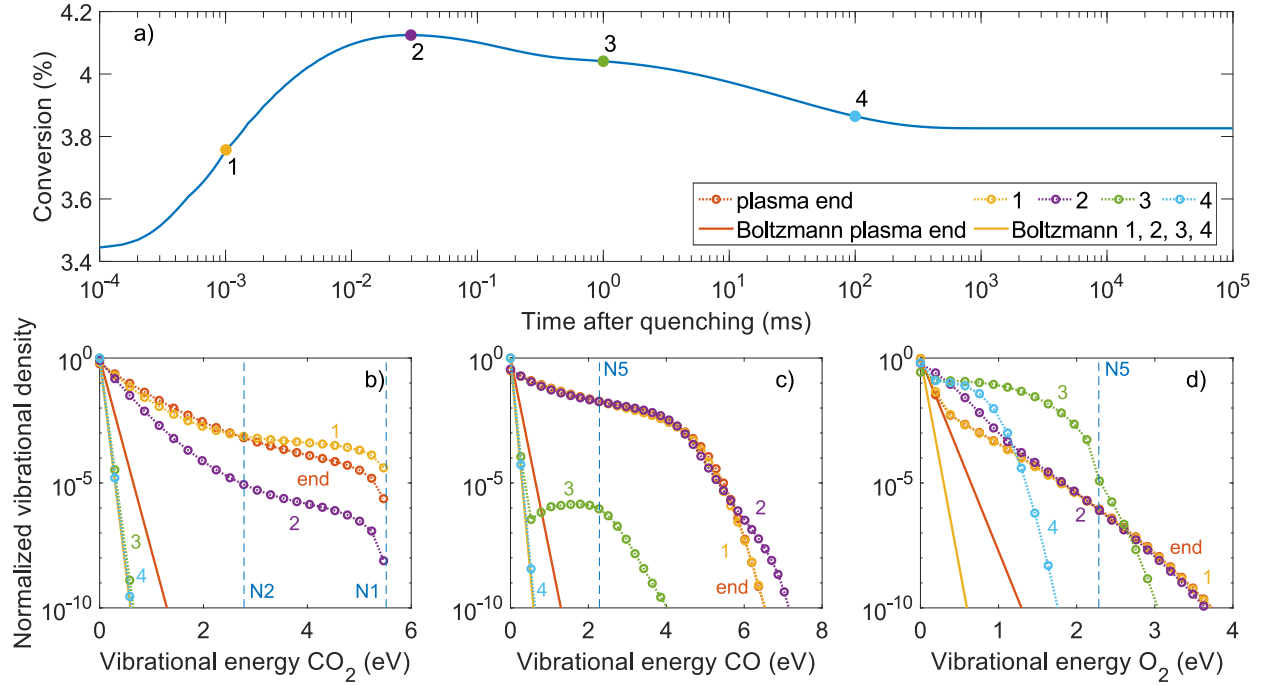
Figure 8: VDFs of CO_2, CO, and O_2 (bottom panels; b-d), and their corresponding Boltzmann distributions, at the end of a warm plasma with SEI of 0.5 eV/molec. (VT non-equilibrium, weak cooling, c = 10^{-3}) (red), and for different times after instantaneous quenching at the plasma end (1 to 4). The different time points are indicated on a plot of the conversion as a function of time (top panel; a). The vertical dashed lines in the bottom panels show the vibrational activation energies (E_a/α) of the dissociation reactions (N1 and N2) (b) and recombination reaction (N5) (c,d).

In fig. 8, right before quenching (i.e. at the plasma end), the higher vibrational levels of all three molecules already have a large overpopulation; see red curve; note that this time point is not indicated in the upper panel, because of the logarithmic x-axis. This is consistent with the VT non-equilibrium for SEI below 1 eV/molec. in fig. 1 (a). Upon quenching, the drop in gas temperature results in a faster VV relaxation, and a slower VT relaxation, leading to a higher population of the higher vibrational levels of CO_2, enabling the dissociation reactions N1 and N2. On the other hand, the strong vibrational overpopulation of CO and O_2 also enables the recombination reaction N5 (see fig. 6 and fig. S1 in the SI). Due to the low conversion degree, CO_2 is the dominant molecule in the mixture, and the rise in N1 and N2, fuelled by the overpopulation of the higher vibrational levels of CO_2, is dominant over the rise in recombination reaction N5. However, the VDF of

CO_2 depopulates much faster than those of CO and O_2, explaining why the fast increase in conversion is followed by a slow drop (point 2, purple curve in fig. 8, and fig. S1 in the SI). After 1 ms (time-point 3, green curve in fig. 8), the higher vibrational levels of CO and O_2 exhibit no overpopulation anymore, and the recombination reaction N5 is no longer important (fig. S1 in the SI). The resulting drop in CO_2 conversion is a result of reaction N4, which has a low activation energy, and does not need vibrational energy to take place.
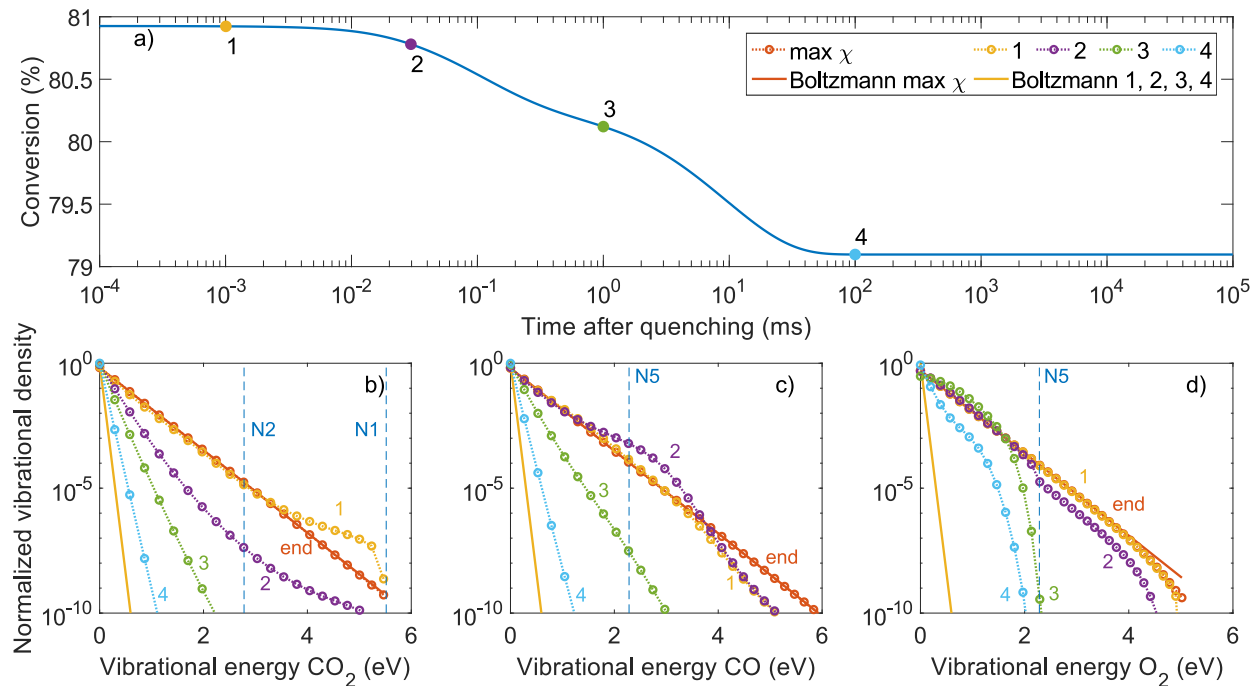

Figure 9: VDFs of CO_2, CO, and O_2 (bottom panels; b-d), and their corresponding Boltzmann distributions, at the end of a warm plasma with SEI of 4 eV/molec. (VT equilibrium, weak cooling; c = 10^{-3}) (red), and for different times after instantaneous quenching at maximum conversion (1 to 4). The different time points are indicated on a plot of the conversion as a function of time (top panel; a). The vertical dashed lines in the bottom panels show the vibrational activation energies (E_a/α) of the dissociation reactions (N1 and N2) (b) and recombination reaction (N5) (c,d).

In fig. 9, the VDFs of the three molecules follow the Boltzmann distribution, since VT equilibrium was established at the plasma end (fig. 1 (a)), and quenching occurs some time after the plasma. Due to the high gas temperature, the distribution of the higher vibrational levels is elevated, but not overpopulated compared to a Boltzmann distribu-

tion. Right after quenching, the Boltzmann distribution drops due to the drop in gas temperature, but the VDFs remain close to the Boltzmann distributions before quenching (see yellow curves; time point 1 in fig. 9). A VT non-equilibrium is therefore created by quenching. Similar to fig. 8, the higher levels of CO_2 are somewhat overpopulated due to the increased VV relaxation. While the vibrational temperature, after quenching, of about 3050 K is very similar to the vibrational temperature of fig. 8 (i.e. 3500 K), the overpopulation of the higher and intermediate levels is much lower. Indeed, due to the much lower population of these levels in fig. 9, VV relaxation requires a longer time to significantly populate the higher vibrational levels, since the energy has to come from the lowest levels. This gives more time for VT relaxation to depopulate the VDF. Also, the conversion degree is much higher, so there is less CO_2 to dissociate, and the recombination reactions are more prominent (fig. S2 of the SI), counteracting the eventual rise in CO_2 dissociation, yielding a net drop in conversion (upper panel of fig. 9). Similarly to fig. 8, the VDFs of CO and O_2 remain populated for a longer time, so recombination reaction N5 is active for a longer time (time point 2, purple curves, and fig. S2 in the SI). Due to the higher concentration of CO and O_2, this results in a higher recombination, and a bigger drop in CO_2 conversion with respect to fig. 8.

For completeness, fig. S7 in the SI illustrates the VDFs of CO_2, CO, and O_2 for a VT non-equilibrium cold plasma at SEI of 4 eV/molec. (i.e. strong cooling; c = 10^3), that is quenched at the plasma end (cf. red curve in fig. 5).

3.6   Effect of Different Quenching Cooling Rates

In previous sections, we discussed the effect of instantaneous quenching. This is the ideal case, but in reality, the gas cooling will not be instantaneous. Therefore, we discuss here the effect of different cooling rates (i.e. different cooling constants c_2 in eq. 9) on the CO_2 conversion, for warm plasmas, i.e. weak initial cooling ($c_1 = 10^{-3}$).

Fig. 10 illustrates the time-evolution of the CO_2 conversion and gas temperature in

the afterglow, for different cooling rates, for a warm non-equilibrium plasma with SEI of 0.5 eV/molec. that is quenched at the plasma end (cf. fig. 3 (a)).
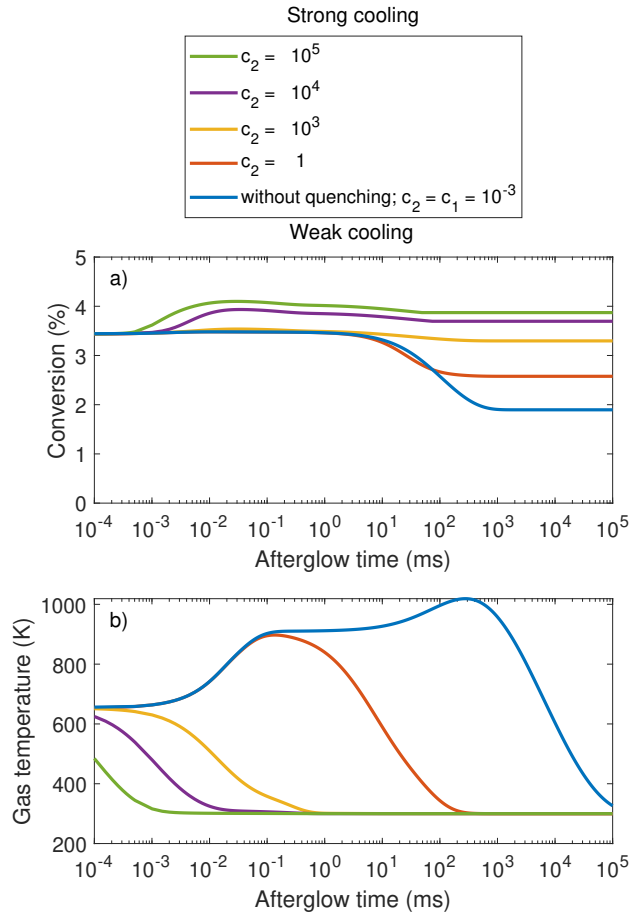

Figure 10: Time-evolution of the CO_2 conversion (a) and gas temperature (b), for different cooling rates in the afterglow, for a VT non-equilibrium plasma with SEI of 0.5 eV/molec. that is quenched at the plasma end. The plasma is initially subjected to weak cooling (c_1 = 10^{-3}), i.e. warm plasma. The cooling constants c_2 in the afterglow are indicated in the legend.

Without quenching (i.e., weak cooling in the afterglow; $c_2 = c_1 = 10^{-3}$), the gas temperature continues to rise in the afterglow (up to about 0.3 s) due to VT relaxation and recombination reactions.

Upon increasing c_2, the gas temperature drops faster (cf. fig. 10 (b)). Hence, recombination becomes less important, resulting in a higher final CO_2 conversion (cf. fig. 10 (a)). For a cooling constant $c_2 \geq 10^4$, the gas temperature reduces to 300 K within 10 μs (or

28

less), and super-ideal quenching becomes apparent (cf. fig. 10). Without quenching ($c_2 = c_1$), VT relaxation quickly depopulates the highest vibrational levels in the afterglow. Fig. S8 in the SI shows that the VDF of CO_2 is in equilibrium within 100 µs after the plasma end. If the cooling rate is high enough ($c_2 \geq 10^4$), the gas temperature drops faster than the VDF can relax. This limits the drop in, or even enhances, the overpopulation of the higher vibrational levels of CO_2, thus increasing the dissociation rates, as the CO_2 vibrational energy can overcome the high activation energy of the dissociation reactions N1 and N2.

Fig. 11 depicts the time-evolution of the CO_2 conversion and gas temperature in the afterglow, for different cooling constants, for a VT equilibrium warm plasma with SEI of 4 eV/molec. that is quenched at maximum conversion (cf. fig. 3 (b)).

In this case, the gas temperature gets high enough to allow for thermal dissociation of CO_2, even after the plasma end. However, due to slow gas cooling, the recombination reactions reduce the CO_2 conversion significantly (cf. fig. 11 (a,b)). Upon higher cooling rate, the final CO_2 conversion increases. Note that the maximum conversion is not reached with maximum cooling rate. Indeed, when the cooling constant rises from 100 to 1000, the conversion slightly decreases (see inset in fig. 11 (a)). This is due to VV relaxation that populates the higher vibrational levels of CO and O_2 at lower gas temperatures (fig. 9), so that they can overcome the high activation energy of the recombination reaction N5. The effect is however minor, and in general, we can conclude that for warm plasma conditions (i.e. weak initial cooling) higher cooling rates yield a higher final CO_2 conversion, either due to super-ideal quenching, further enhancing the CO_2 conversion (fig. 10) or simply by freezing the CO_2 conversion, because the recombination reactions become negligible at low gas temperatures (fig. 11).
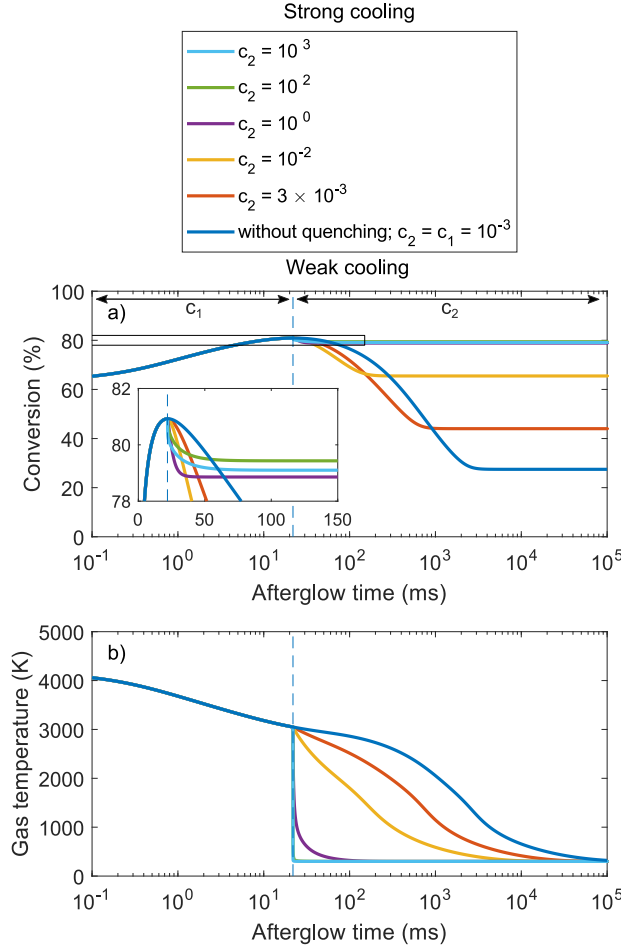
Figure 11: Time-evolution of the CO_2 conversion (a) and gas temperature (b), for different cooling rates, for a VT equilibrium plasma with SEI of 4 eV/molec. that is quenched at maximum CO_2 conversion. The plasma is initially subjected to weak cooling ($c_1 = 10^{-3}$), i.e. warm plasma. The cooling constants c_2 in the afterglow are indicated in the legend.

3.7 Comparison of Plasma-Based and Thermal CO_2 Conversion at Different SEI Values and Gas Temperatures, and Effect of Instantaneous Quenching

Fig. 12 illustrates the CO_2 conversion and energy efficiency as a function of SEI for a warm plasma ($c = 10^{-3}$), as well as for the purely thermal process, in which the same power is applied as heat, as explained in section 2.3, both with and without quenching at maximum CO_2 conversion. The maximum gas temperature in both cases is shown on the
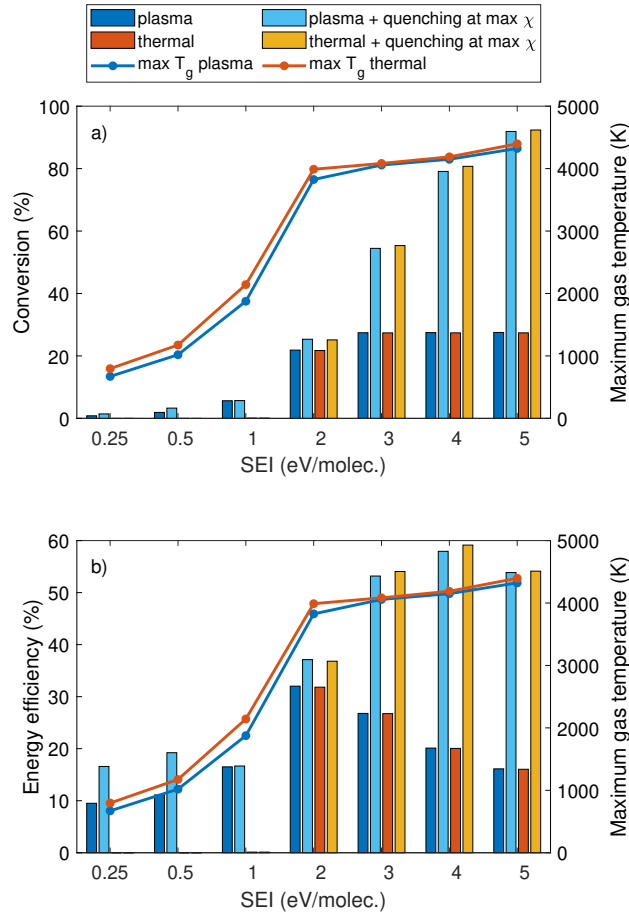
30

right axis.

Figure 12: CO_2 conversion (a; left axis) and energy efficiency (b; left axis) and maximum gas temperature (right axis) as a function of SEI, for a warm plasma (i.e. weak cooling; c = 10^{-3}) and pure thermal conversion, with and without quenching at maximum conversion.

For SEI values ≤ 1 eV/molec., the maximum gas temperature is too low for thermal dissociation of CO_2. The thermal process therefore shows negligible conversion, while the plasma process exhibits a conversion of about 0.8-5.6 %, corresponding to an energy efficiency of $9.5 - 16.5$ %, mostly attributed to vibrational-induced dissociation, but also electron impact dissociation.

For SEI ≥ 2 eV/molec., the conversion and energy efficiency of the thermal process rise, and they are similar to the plasma process, both with and without quenching. In addition, the maximum gas temperatures are also very comparable, due to the high VT relaxation that results in a VT equilibrium (see fig. 1). Upon quenching, a similar be-

havior takes place because in both cases a VT non-equilibrium is created, since the VDF is "frozen" in its Boltzmann distribution from right before quenching (see fig. 9). Similarly as in the plasma quenching case, the conversion degree slightly drops due to the higher concentration of CO and O_2, promoting a higher recombination (see figs. 3 b and 9). However, at high SEI, the conversion and energy efficiency of the quenched thermal case perform slightly better than that of the plasma case. This is because the power goes directly to the neutral species, while in the plasma case, inefficient processes like electron impact dissociation still play a role (see figs. 6 and 7). Without quenching, the final CO_2 conversion remains constant at 27-28 %, due to the slow cooling, which promotes recombination reactions.

In fig. 13, we plot the CO_2 conversion and energy efficiency (left axis) as a function of cooling constant (c), i.e., mimicking warm and cold plasmas at different temperatures (see curves and right axis), for plasma-based and thermal conversion, both with an SEI of 4 eV/molec, and both without quenching and for instantaneous quenching at maximum conversion (i.e., the gas temperature drops immediately to 300 K).
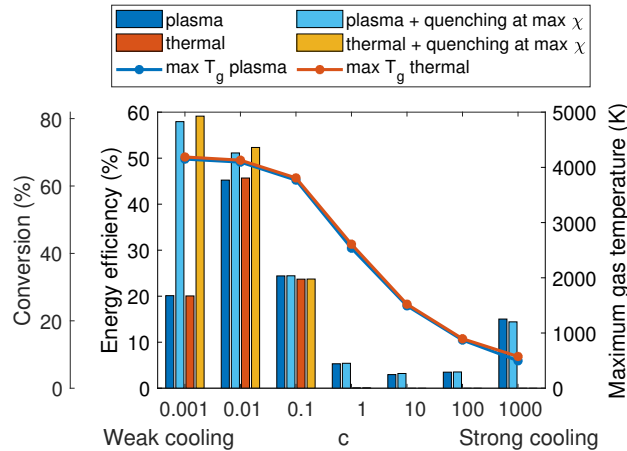

Figure 13: Energy efficiency and CO_2 conversion (left axis), and maximum gas temperature (right axis) as a function of cooling constant c for the plasma and purely thermal process, with SEI of 4 eV/molec., without quenching and with instantaneous quenching at maximum conversion.

At weak cooling (c = 10^{-3}), corresponding to a maximum gas temperature of 4150-

4200 K, quenching reaches the highest conversion of 79 % and 81 %, corresponding to an energy efficiency of 58% and 59%, for the plasma and purely thermal case, respectively. At these high temperatures, the conversion is mostly thermal. The difference between the quenching and no quenching is also high, since the slow drop in gas temperature without quenching is detrimental for the conversion (see also fig. 2). With increasing cooling constant c, the maximum gas temperature decreases, leading to lower thermal conversion. Also the difference with and without quenching decreases, as the higher afterglow cooling also leaves less time for recombination. Note that the higher conversion is already significant for moderate cooling (c = 0.01 vs 10^{-3}), corresponding to low reduction in the maximum gas temperature, as the recombination in the afterglow typically occurs over a long time (order of 1 s; see fig. 2). When the cooling c reaches 1, the maximum gas temperature is around 2500 K, which is too low for (substantial) thermal dissociation. Therefore, the thermal CO_2 conversion and energy efficiency become negligible. The plasma-based CO_2 conversion and energy efficiency also drop. Indeed, while the gas temperature is too low for substantial thermal dissociation, it is still high enough for considerable VT relaxation, which prevents an efficient vibrational-induced dissociation. This VT relaxation becomes less important upon even stronger cooling, leading to higher vibrational induced dissociation, and a subsequent rise in final CO_2 conversion and energy efficiency, for c $\geq$ 100. These conditions correspond to cold VT non-equilibrium plasmas, where quenching does not enhance the CO_2 conversion or energy efficiency (cf. fig. 5).

It must be realized that the exact values of conversion and energy efficiency are subject to uncertainties, as mentioned in section 2.2, and should thus be considered with caution, but the trends predicted by the model, for the effect of quenching and the comparison between plasma-based and thermal conversion should be reliable. Indeed, our modeling results are in reasonable agreement with the model of Kotov and Koelman, predicting maximum energy efficiencies of about 40 % at 4 eV/molec. in MW plasmas at comparable pressure,[42] and also stressing the dominant role of thermal conversion. den Harder

et al.[19] and Bongers et al.[21] reported experimental energy efficiencies up to 48 % for gas temperatures between 3500-4000 K, at intermediate pressure. In addition, experiments revealed that quenching in the afterglow can enhance the energy efficiency to values around 50 %.[17,21] However, exact comparison with these experimental results is difficult, due to possible deviations in pressure, ionization degree and reduced electric field, and because of limitations to the 0D model,[61] like not describing transport phenomena, and assuming spatial homogeneity. These transport phenomena might play an eminent role in facilitating the quenching process.[39]

3.8 Quenching at Higher Ionization Degree

In the previous sections, we considered an ionization degree of 10^{-6}. In contracted MW plasmas, the ionization degree can be much higher, up to 10^{-4}.[40] Therefore, we show here the evolution of the CO_2 conversion and energy efficiency as a function of SEI, for an ionization degree of 10^{-4}. The reduced electric field is kept at 50 Td.
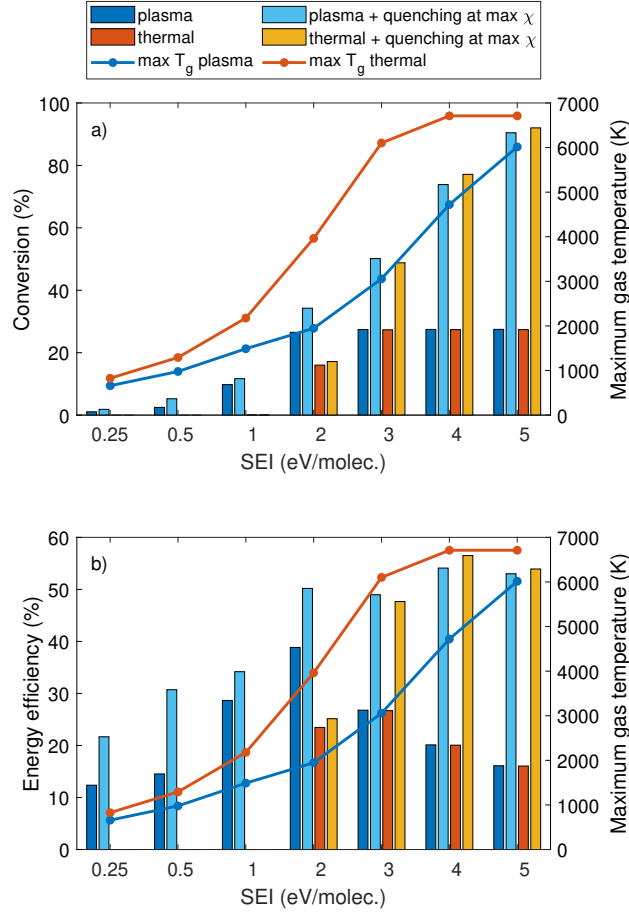
Figure 14: CO_2 conversion (a; left axis) and energy efficiency (b; left axis) and maximum gas temperature (right axis) as a function of SEI for the plasma and purely thermal process, with and without quenching, for an ionization degree of 10^{-4}, and weak cooling (c $= 10^{-3}$). The reduced electric field is 50 Td.

In fig. 14 we plot the conversion and energy efficiency (left axis) as a function of SEI, for the plasma and thermal process, at low cooling (c = 10^{-3}). The gas is instantaneously quenched at maximum conversion, and the maximum gas temperature is shown for both cases (right axis). When comparing fig. 14 with fig. 12, we can see that the conversion and energy efficiency are slightly higher at this higher ionization degree for SEI values ≤ 2 eV/molec. For SEI values ≤ 1 eV/molec. the temperature is too low for thermal conversion. Even at 2 eV/molec., the plasma-based conversion and energy efficiency are higher than for thermal conversion, both with and without quenching, since a higher ionization degree results in more electron impact reactions, including more electron impact

35

vibrational excitation, and consequently also in more vibrational-induced dissociation.[29] Similar to the lower ionization degree of 10^{-6}, the highest conversions and energy efficiencies are again found for the higher SEI values (see also fig. 12). Note also that the maximum gas temperature for these higher SEIs is larger than for a lower ionization degree (see fig. 12). This is also observed in experiments.[62]

For an SEI of 3-5 eV/molec., the conversions and energy efficiencies are very similar for plasma and thermal conversion, both with and without quenching. However, the maximum gas temperature is much lower for the plasma process than for the thermal process. This is because more energy goes to the vibrational levels at higher ionization degree, resulting in more vibrational-induced dissociation. Despite the difference in maximum gas temperature, and the fact that more of the plasma-based CO_2 conversion takes place through vibrational-induced dissociation, the final CO_2 conversion and hence energy efficiency are similar for the plasma and thermal process. The energy efficiencies at these higher SEI values are very similar to the ones at lower ionization degree (see fig. 12).

3.9   Quenching at Higher Reduced Electric Field

All previous results were obtained for a reduced electric field of 50 Td. As this value may be quite low for practical MW plasmas, we present here the evolution of CO_2 conversion and energy efficiency as a function of SEI, for a reduced electric field of 100 Td, again for a low cooling (c = 10^{-3}), and an ionization degree of 10^{-6}, and for both the plasma and thermal process, with and without quenching (instantaneous quenching at maximum conversion). The maximum gas temperature is shown for both cases on the right axis.

Fig. 15 shows a similar evolution with increasing SEI as at lower E/N (see fig. 12). At low SEI values (SEI = 0.25 − 1 eV/molec.), the plasma exhibits a low conversion and energy efficiency, and there is no thermal dissociation. At SEI = 2 eV/molec. the plasma process is less efficient than the thermal process, both with and without quenching. The
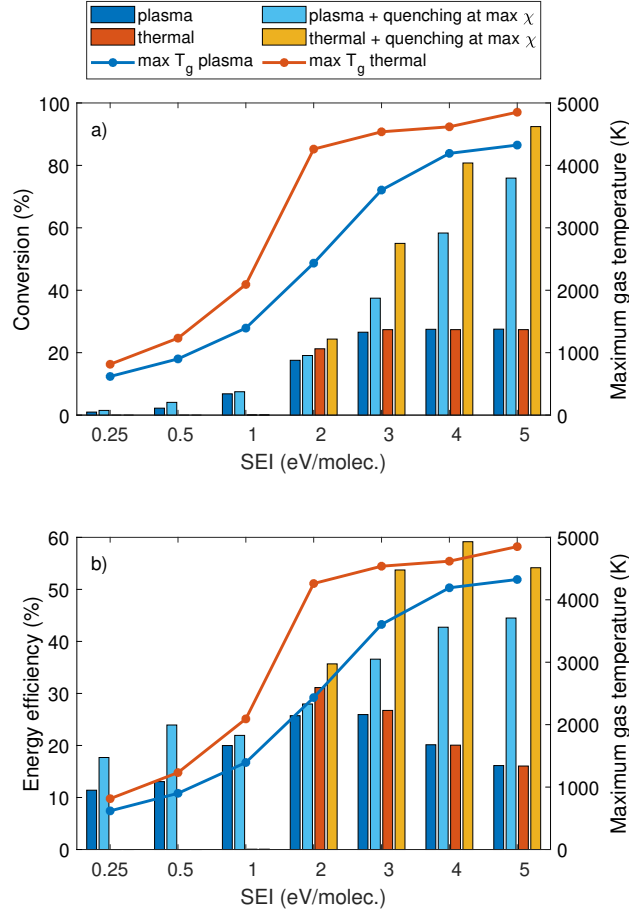
Figure 15: CO_2 conversion (a; left axis) and energy efficiency (b; left axis) and maximum gas temperature (right axis) as a function of SEI for the plasma and purely thermal process, with and without quenching, for an reduced electric field of 100 Td, and weak cooling (c = 10^{-3}). The ionization degree is 10^{-6}.

same applies to higher SEI values upon quenching. This is because the higher reduced electric field makes electron impact dissociation more prominent, but the latter is less energetically favourably, explaining the lower energy efficiency than for pure thermal conversion. At higher SEI values (SEI = 3 – 5 eV/molec.), the plasma and thermal process without quenching become equally efficient, because the slow drop in gas temperature reduces the CO_2 conversion to a value of 27-28 %.

4 Conclusions

We demonstrated the potential of quenching for plasma-based CO_2 conversion, by means of chemical kinetics modelling. We consider so-called warm plasmas at a pressure of 100 mbar, an ionization degree of 10^{-6} and a reduced electric field of 50 Td, but our model predicts that the trends are the same at higher ionization degree (10^{-4}) and reduced electric field (100 Td).

We calculated the gas and vibrational temperature, and the CO_2 conversion, as a function of time in the plasma, at weak and strong cooling, mimicking warm and cold plasma conditions, respectively. At weak cooling, high conversion degrees were reached for large SEI values (i.e., up to 96 % at SEI = 5 eV/molec.), due to the high gas temperature (~ 4000 K), leading to VT equilibrium and thus thermal conversion. However, without additional cooling in the afterglow, the conversion drops dramatically, due to the backward (recombination) reactions, leading to a low overall CO_2 conversion of 27 – 28 %.

We examined the effect of quenching for warm and cold plasma conditions, and we explained the results based on the dissociation and recombination reactions and the VDFs of the CO_2, CO and O_2 molecules. For warm plasma conditions at low SEI, yielding VT non-equilibrium, our model predicts it is best to quench at the plasma end. In this case, quenching can even further enhance the dissociation by the reactions ($CO_2 + M \rightarrow CO + O + M$ and $CO_2 + O \rightarrow CO + O_2$), due to the overpopulation of the CO_2 vibrational levels, which helps to overcome the activation energy of these reactions. This process is called "super-ideal quenching". For cold plasma conditions at high SEI, which also result in VT non-equilibrium, quenching also enhances the dissociation, but it promotes the recombination reactions even more, leading to a lower final CO_2 conversion. For warm plasma conditions at high SEI, yielding VT equilibrium, the high gas temperature enhances the CO_2 conversion even after the plasma, so it is more favourable to quench at maximum conversion. Upon fast quenching, both dissociation and recombination reactions stop, so the CO_2 conversion is frozen, leading to a much higher final CO_2 conversion and overall

energy efficiency than without quenching (even up to a factor three enhancement).

We also evaluated the effect of different cooling rates in the afterglow, demonstrating overall the importance of fast cooling, although at high SEI values we also have to account for overpopulation of the higher vibrational levels of CO, which can overcome the activation energy of the recombination reaction, therefore leading to more recombination, resulting in a slight drop in the overall conversion.

Finally, we compared the performance of plasma-based CO_2 conversion with purely thermal conversion, for different SEI values and for warm (i.e. low cooling) and cold (i.e. high cooling) plasmas, as well as the effect of quenching, on both the CO_2 conversion and energy efficiency. For warm plasmas at SEI $\geq$ 2 eV/molec., yielding gas temperatures of 3000-4000 K, the plasma-based conversion is mostly thermal, and quenching can enhance the conversion and energy efficiency by up to a factor three. For low SEI plasmas at lower temperatures, when thermal conversion is negligible, the overall conversion and energy efficiency are quite low, and in addition, quenching becomes less efficient. For cold plasmas in VT non-equilibrium at high SEI, quenching can even decrease the final CO_2 conversion.

In summary, our model provides interesting insights in how quenching can improve the CO_2 conversion and energy efficiency for various plasma conditions and cooling conditions. We showed that the highest conversion and energy efficiency can be reached for thermal conversion, at high gas temperatures in the plasma, followed by fast quenching. Such quenching can be realized when expanding the flow after the plasma, as demonstrated experimentally,[17,21] but it may also be accomplished by mixing with a cold gas. In addition, the quenching might be combined with heat recovery, for preheating the gas entering the plasma reactor, so that less plasma power is wasted for gas heating, and all the power could be used for the conversion process.

Acknowledgement

Supporting Information Available

The supporting information is available free of charge and contains:

- Reactions included in the models as well as their rate coefficients or cross sections

- Scaling laws

- Effect of instantaneous quenching on the evolution of the dissociation and recombination rates for a plasma subjected to low cooling

- Effect of instantaneous quenching on the O atom density

- Effect of instantaneous quenching on the dissociation and recombination rates for a plasma subjected to strong cooling

- Effect of instantaneous quenching on the VDFs of CO_2, CO, and O_2 for a plasma subjected to strong cooling

- Relaxation time of the CO_2 VDF at low SEI

References

(1) Norhasyima, R.; Mahlia, T. Advances in CO_2 utilization technology: A patent landscape review. *J. CO_2 Util.* **2018**, *26*, 323–335.

(2) Fridman, A. *Plasma Chemistry*; Cambridge University Press: New York, USA, 2008.

(3) Bogaerts, A.; Neyts, E. C. Plasma Technology: An Emerging Technology for Energy Storage. *ACS Energy Lett.* **2018**, *3*, 1013–1027.

(4) Snoeckx, R.; Bogaerts, A. Plasma Technology - a Novel Solution for CO_2 Conversion? *Chem. Soc. Rev.* **2017**, *46*, 5805–5863.

(5) Mei, D.; Zhu, X.; He, Y.-L.; Yan, J. D.; Tu, X. Plasma-assisted conversion of CO_2 in a dielectric barrier discharge reactor: understanding the effect of packing materials. *Plasma Sources Sci. Technol.* **2014**, *24*, 015011.

(6) Mei, D.; Tu, X. Atmospheric Pressure Non-Thermal Plasma Activation of CO_2 in a Packed-Bed Dielectric Barrier Discharge Reactor. *ChemPhysChem* **2017**, *18*, 3253–3259.

(7) Belov, I.; Paulussen, S.; Bogaerts, A. Appearance of a Conductive Carbonaceous Coating in a CO_2 Dielectric Barrier Discharge and its Influence on the Electrical Properties and the Conversion Efficiency. *Plasma Sources Sci. Technol.* **2016**, *25*, 015023.

(8) Uytdenhouwen, Y.; Van Alphen, S.; Michielsen, I.; Meynen, V.; Cool, P.; Bogaerts, A. A Packed-bed DBD Micro Plasma Reactor for CO_2 Dissociation: Does Size Matter? *Chem. Eng. J.* **2018**, *348*, 557–568.

(9) Michielsen, I.; Uytdenhouwen, Y.; Pype, J.; Michielsen, B.; Mertens, J.; Reniers, F.; Meynen, V.; Bogaerts, A. CO_2 Dissociation in a Packed Bed DBD Reactor: First Steps Towards a Better Understanding of Plasma Catalysis. *Chem. Eng. J.* **2017**, *326*, 477–488.

(10) Yu, Q.; Kong, M.; Liu, T.; Fei, J.; Zheng, X. Characteristics of the Decomposition of CO_2 in a Dielectric Packed-Bed Plasma Reactor. *Plasma Chem. Plasma Process.* **2012**, *32*, 153–163.

(11) Paulussen, S.; Verheyde, B.; Tu, X.; De Bie, C.; Martens, T.; Petrovic, D.; Bogaerts, A.; Sels, B. Conversion of Carbon Dioxide to Value-Added Chemicals in Atmospheric Pressure Dielectric Barrier Discharges. *Plasma Sources Sci. Technol.* **2010**, *19*, 034015 1–6.

(12) Aerts, R.; Somers, W.; Bogaerts, A. Carbon Dioxide Splitting in a Dielectric Barrier Discharge Plasma: A Combined Experimental and Computational Study. *ChemSusChem* **2015**, *8*, 702–716.

(13) Wang, W.; Mei, D.; Tu, X.; Bogaerts, A. Gliding Arc Plasma for CO_2 Conversion: Better Insights by a Combined Experimental and Modelling Approach. *Chem. Eng. J.* **2017**, *330*, 11–25.

(14) Nunnally, T.; Gutsol, K.; Rabinovich, A.; Fridman, A.; Gutsol, A.; Kemoun, A. Dissociation of CO_2 in a Low Current Gliding Arc Plasmatron. *J. Phys. D: Appl. Phys.* **2011**, *44*, 274009.

(15) Ramakers, M.; Trenchev, G.; Heijkers, S.; Wang, W.; Bogaerts, A. Gliding Arc Plasmatron: Providing an Alternative Method for Carbon Dioxide Conversion. *ChemSusChem* **2017**, *10*, 2642–2652.

(16) Belov, I.; Vermeiren, V.; Paulussen, S.; Bogaerts, A. Carbon Dioxide Dissociation in a Microwave Plasma Reactor Operating in a Wide Pressure Range and Different Gas Inlet Configurations. *J. CO_2 Util.* **2018**, *24*, 386–397.

(17) Goede, A. P. CO_2 neutral fuels. *EPJ Web of Conferences* **2018**, *189*.

(18) van Rooij, G. J.; van den Bekerom, D. C. M.; den Harder, N.; Minea, T.; Berden, G.; Bongers, W. A.; Engeln, R.; Graswinckel, M. F.; Zoethout, E.; van de Sanden, M. C. M. Taming microwave plasma to beat thermodynamics in CO_2 dissociation. *Faraday Discuss.* **2015**, *183*, 233–248.

(19) den Harder, N.; van den Bekerom, D. C. M.; Al, R. S.; Graswinckel, M. F.; Palomares, J. M.; Peeters, F. J. J.; Ponduri, S.; Minea, T.; Bongers, W. A.; van de Sanden, M. C. M. et al. Homogeneous CO_2 Conversion by Microwave Plasma: Wave Propagation and Diagnostics. *Plasma Processes Polym.* **2017**, *14*, 1600120.

(20) van den Bekerom, D. C. M.; Linares, J. M. P.; Verreycken, T.; van Veldhuizen, E. M.; Nijdam, S.; Berden, G.; Bongers, W. A.; van de Sanden, M. C. M.; van Rooij, G. J. The Importance of Thermal Dissociation in CO_2 Microwave Discharges Investigated by Power Pulsing and Rotational Raman Scattering. *Plasma Sources Sci. Technol.* **2019**, *28*, 055015.

(21) Bongers, W.; Bouwmeester, H.; Wolf, B.; Peeters, F.; Welzel, S.; van den Bekerom, D.; den Harder, N.; Goede, A.; Graswinckel, M.; Groen, P. W. et al. Plasma-driven dissociation of CO_2 for fuel synthesis. *Plasma Processes Polym.* **2017**, *14*, 1600126.

(22) Wang, J.-Y.; Xia, G.-G.; Huang, A.; Suib, S. L.; Hayashi, Y.; Matsumoto, H. CO_2 Decomposition Using Glow Discharge Plasmas. *J. Catal.* **1999**, *185*, 152–159.

(23) Trenchev, G.; Nikiforov, A.; Wang, W.; Kolev, S.; Bogaerts, A. Atmospheric Pressure Glow Discharge for CO_2 Conversion: Model-based Exploration of the Optimum Reactor Configuration. *Chem. Eng. J.* **2019**, *362*, 830–841.

(24) Martini, L. M.; Gatti, N.; Dilecce, G.; Scotoni, M.; Tosi, P. Laser Induced Fluorescence in Nanosecond Repetitively Pulsed Discharges for CO_2 Conversion. *Plasma Phys. Controlled Fusion* **2018**, *60*, 014016.

(25) Martini, L. M.; Lovascio, S.; Dilecce, G.; Tosi, P. Time-Resolved CO_2 Dissociation in a Nanosecond Pulsed Discharge. *Plasma Chem. Plasma Process.* **2018**, *38*, 707–718.

(26) Moss, M. S.; Yanallah, K.; Allen, R. W. K.; Pontiga, F. An Investigation of CO_2 Splitting Using Nanosecond Pulsed Corona Discharge: Effect of Argon Addition on CO_2 Conversion and Energy Efficiency. *Plasma Sources Sci. Technol.* **2017**, *26*, 035009.

(27) Heijkers, S.; Martini, L. M.; Dilecce, G.; Tosi, P.; Bogaerts, A. Nanosecond Pulsed Discharge for CO_2 Conversion: Kinetic Modeling To Elucidate the Chemistry and Improve the Performance. *J. Phys. Chem. C* **2019**, *123*, 12104–12116.

(28) Kozák, T.; Bogaerts, A. Splitting of CO_2 by Vibrational Excitation in Non-Equilibrium Plasmas: a Reaction Kinetics Model. *Plasma Sources Sci. Technol.* **2014**, *23*, 045004.

(29) Berthelot, A.; Bogaerts, A. Pinpointing Energy Losses in CO_2 Plasmas - Effect on CO_2 Conversion. *J. CO_2 Util.* **2018**, *24*, 479–499.

(30) Pietanza, L. D.; Colonna, G.; D'Ammando, G.; Capitelli, M. Time-Dependent Coupling of Electron Energy Distribution Function, Vibrational Kinetics of the Asymmetric Mode of CO_2 and Dissociation, Ionization and Electronic Excitation Kinetics under Discharge and Post-Discharge Conditions. *Plasma Phys. Controlled Fusion* **2017**, *59*, 014035.

(31) Berthelot, A.; Bogaerts, A. Modeling of CO_2 Splitting in a Microwave Plasma: How to Improve the Conversion and Energy Efficiency. *J. Phys. Chem. C* **2017**, *121*, 8236–8251.

(32) Klarenaar, B. L. M.; Engeln, R.; van den Bekerom, D. C. M.; van de Sanden, M. C. M.; Morillo-Candas, A. S.; Guaitella, O. Time Evolution of Vibrational Temperatures in a CO_2 Glow Discharge Measured with Infrared Absorption Spectroscopy. *Plasma Sources Sci. Technol.* **2017**, *26*, 115008.

(33) Klarenaar, B. L. M.; Morillo-Candas, A. S.; Grofulović, M.; van de Sanden, M. C. M.; Engeln, R.; Guaitella, O. Excitation and relaxation of the asymmetric stretch mode of CO_2 in a pulsed glow discharge. *Plasma Sources Sci. Technol.* **2019**, *28*, 035011.

(34) Silva, T.; Britun, N.; Godfroid, T.; van der Mullen, J.; Snyders, R. Study of Ar and Ar-CO_2 Microwave Surfaguide Discharges by Optical Spectroscopy. *J. Appl. Phys.* **2016**, *119*, 173302.

(35) Silva, T.; Grofulović, M.; Klarenaar, B. L. M.; Morillo-Candas, A. S.; Guaitella, O.; Engeln, R.; Pintassilgo, C. D.; Guerra, V. Kinetic study of low-temperature CO_2 plasmas under non-equilibrium conditions. I. Relaxation of vibrational energy. *Plasma Sources Sci. Technol.* **2018**, *27*, 015019.

(36) Pietanza, L. D.; Colonna, G.; D'Ammando, G.; Laricchiuta, a.; Capitelli, M. Vibrational Excitation and Dissociation Mechanisms of CO_2 under Non-Equilibrium Discharge and Post-Discharge Conditions. *Plasma Sources Sci. Technol.* **2015**, *24*, 042002.

(37) Pietanza, L. D.; Colonna, G.; D'Ammando, G.; Laricchiuta, A.; Capitelli, M. Electron Energy Distribution Functions and Fractional Power Transfer in "Cold" and Excited CO_2 Discharge and Post Discharge Conditions. *Phys. Plasma* **2016**, *23*.

(38) Heijkers, S.; Bogaerts, A. CO_2 Conversion in a Gliding Arc Plasmatron: Elucidating the Chemistry through Kinetic Modeling. *J. Phys. Chem. C* **2017**, *121*, 22644–22655.

(39) Wolf, A. J.; Peeters, F. J. J.; Groen, P. W. C.; Bongers, W. A.; van de Sanden, M. C. M. CO_2 Conversion in Nonuniform Discharges: Disentangling Dissociation and Recombination Mechanisms. *J. Phys. Chem. C* **2020**, in press.

(40) Wolf, A. J.; Righart, T. W. H.; Peeters, F. J. J.; Groen, P. W. C.; van de Sanden, M. C. M.; Bongers, W. A. Characterization of CO_2 microwave plasma based on the phenomenon of skin-depth-limited contraction. *Plasma Sources Sci. Technol.* **2019**, *28*, 115022.

(41) Wolf, A. J.; Righart, T. W. H.; Peeters, F. J. J.; Bongers, W. A.; van de Sanden, M. C. M. Implications of thermo-chemical instability on the contracted modes in CO_2 microwave plasmas. *Plasma Sources Sci. Technol.* **2020**, *29*, 025005.

(42) Kotov, V.; Koelman, P. M. J. Plug flow reactor model of the plasma chemical conversion of CO_2. *Plasma Sources Sci. Technol.* **2019**, *28*, 095002.

(43) Wilcox, D. C. *Turbulence Modeling for CFD*, 3rd ed.; DCW industries Inc.: La Canada, USA, 2006.

(44) Trenchev, G.; Kolev, S.; Wang, W.; Ramakers, M.; Bogaerts, A. CO_2 Conversion in a Gliding Arc Plasmatron: Multidimensional Modeling for Improved Efficiency. *J. Phys. Chem. C* **2017**, *121*, 24470–24479.

(45) Vermeiren, V.; Bogaerts, A. Supersonic Microwave Plasma: Potential and Limitations for Energy-Efficient CO_2 Conversion. *J. Phys. Chem. C* **2018**, *122*, 25869–25881.

(46) Pancheshnyi, S.; Eismann, B.; Hagelaar, G.; Pitchford, L. Computer code ZDPlasKin. 2008; `http://www.zdplaskin.laplace.univ-tlse.fr`, (accessed September 2017).

(47) Hagelaar, G. J. M.; Pitchford, L. C. Solving the Boltzmann Equation to Obtain Electron Transport Coefficients and Rate Coefficients for Fluid Models. *Plasma Sources Sci. Technol.* **2005**, *14*, 722–733.

(48) Koelman, P.; Heijkers, S.; Tadayon Mousavi, S.; Graef, W.; Mihailova, D.; Kozák, T.; Bogaerts, A.; van Dijk, J. A Comprehensive Chemical Model for the Splitting of CO_2 in Non-Equilibrium Plasmas. *Plasma Processes Polym.* **2017**, *14*, 1600155.

(49) Berthelot, A.; Bogaerts, A. Modeling of CO_2 Plasma: Effect of Uncertainties in the Plasma Chemistry. *Plasma Sources Sci. Technol.* **2017**, *26*, 115002.

(50) Kozák, T.; Bogaerts, A. Evaluation of the Energy Efficiency of CO_2 Conversion in Microwave Discharges using a Reaction Kinetics Model. *Plasma Sources Sci. Technol.* **2015**, *24*, 015024.

(51) Vermeiren, V.; Bogaerts, A. Improving the Energy Efficiency of CO_2 Conversion in Nonequilibrium Plasmas through Pulsing. *J. Phys. Chem. C* **2019**, *123*, 17650–17665.

(52) Phelps, A. V. Phelps Database. `www.lxcat.net`, (accessed September 2014).

(53) Grofulović, M.; Alves, L. L.; Guerra, V. Electron-Neutral Scattering Cross Sections for CO_2: a Complete and Consistent Set and an Assessment of Dissociation. *J. Phys. D: Appl. Phys.* **2016**, *49*, 395207.

(54) Berthelot, A.; Bogaerts, A. Modeling of Plasma-Based CO_2 Conversion: Lumping of the Vibrational Levels. *Plasma Sources Sci. Technol.* **2016**, *25*, 045022.

(55) Itikawa, Y. Cross Sections for Electron Collisions with Carbon Monoxide. *J. Phys. Chem. Ref. Data* **2015**, *44*, 013105.

(56) Britun, N.; Silva, T.; Chen, G.; Godfroid, T.; van der Mullen, J.; Snyders, R. Plasma-assisted CO_2 Conversion: Optimizing Performance via Microwave Power Modulation. *J. Phys. D: Appl. Phys.* **2018**, *51*, 144002.

(57) Silva, T.; Britun, N.; Godfroid, T.; Snyders, R. Optical Characterization of a Microwave Pulsed Discharge used for Dissociation of CO_2. *Plasma Sources Sci. Technol.* **2014**, *23*, 025009.

(58) Guerra, V.; Tatarova, E.; Dias, F. M.; Ferreira, C. M. On the self-consistent modeling of a traveling wave sustained nitrogen discharge. *J. Appl. Phys.* **2002**, *91*, 2648–2661.

(59) Buser, R. G.; Sullivan, J. J. Initial Processes in CO_2 Glow Discharges. *J. Appl. Phys.* **1970**, *41*, 472–479.

(60) van den Bekerom, D. C. M.; van de Steeg, A.; van de Sanden, M. C. M.; van Rooij, G. J. Mode resolved heating dynamics in pulsed microwave CO_2 plasma from laser Raman scattering. *J. Phys. D: Appl. Phys.* **2020**, *53*, 054002.

(61) Hurlbatt, A.; Gibson, A. R.; Schröter, S.; Bredin, J.; Foote, A. P. S.; Grondein, P.; O'Connell, D.; Gans, T. Concepts, Capabilities, and Limitations of Global Models: A Review. *Plasma Processes Polym.* **2017**, *14*, 1600138.

(62) Groen, P. W. C.; Wolf, A. J.; Righart, T. W. H.; van de Sanden, M. C. M.; Peeters, F. J. J.; Bongers, W. A. Numerical model for the determination of the reduced electric field in a CO_2 microwave plasma derived by the principle of impedance matching. *Plasma Sources Sci. Technol.* **2019**, *28*, 075016.

Graphical TOC Entry